To appear in IEEE Transactions on Control Systems Technology

Memory-Element Based Hysteresis: Identification and Compensation of a Piezoelectric Actuator

Nard Strijbosch, *Student, IEEE*, Koen Tiels *Member, IEEE*, and Tom Oomen, *Senior Member, IEEE*

***Abstract*— Hysteresis phenomena can significantly deteriorate the performance when performing servo tasks with piezoelectric actuators. The aim of this paper is to model this nonlinear hysteresis effect and use this model to develop a feedforward controller that compensates for the hysteretic behaviour. Exploiting the dual-pair concept, a connection is established between hysteresis models and general memory elements examplified by the Ramberg-Osgood model. This facilitates both a straightforward identification procedure of a hysteresis model and feedforward controller design. Both the identification procedure and feedforward controller are implemented on a piezoelectric actuator indicating a performance improvement by a factor 3.5.**

***Index Terms*— Feedforward, Hysteresis, Mechatronics, Precision Motion Control,**

I. Introduction

FEEDFOWARD control can effectively compensate for known disturbances, e.g., a reference trajectory, before these affect the system. The feedforward controller often consists of the inverse of an identified model of the system [1], [2]. For instance, in linear mechanical systems, Newton's law $F = ma$ can be used as the inverse of a mass system, the parameter m can easily be determined using a manual tuning approach, see, e.g., [3] for tuning guidelines, and [4] for an automated tuning algorithm.

Feedforward is also successfully applied to compensate for nonlinear effects such as Coulomb friction [5]. Interestingly, the inverse model of Coulomb friction can be uniquely determined regardless of its nonlinear nature. By parameterising the feedforward linear in the parameters, it can be efficiently tuned in a user-friendly manner [3].

Hysteresis can significantly deteriorate the performance, e.g., in systems that exploit piezoelectric actuators. A wide variety of models exist to capture the hysteretic behaviour, including the Ramberg-Osgood model [6], [7], the Maxwell-Slip model [8], the Bouc-Wen model [9], the Preisach model [10], the Coleman-Hodgdon model [11], and the Prandtl-Ishlinskii model [12], [13], see [14] for a comparison.

Nard Strijbosch, Koen Tiels, and Tom Oomen are with the Control Systems Technology Group, Departement of Mechanical Engineering, Eindhoven University of Technology, P.O. Box 513, 5600 MB Eindhoven, The Netherlands, e-mail: n.w.a.strijbosch@tue.nl, k.tiels@tue.nl, t.a.e.oomen@tue.nl. This work is part of the research programme VIDI with project number 15698, which is (partly) financed by the Netherlands Organisation for Scientific Research (NWO).

A key challenge to determine a feedforward controller to compensate for the hysteresis phenomena is non-uniqueness. Hysteresis depends on past inputs, hence inverting the input-output mapping cannot be done in a straight forward manner. Nonetheless, an inverse feedforward has been developed for certain cases of hysteresis models, including, e.g., [15]–[17] for a feedforward controller based on the Prandtl-Ishlinskii model, and [18] for a feedforward controller based on the Preisach model. The identification procedure of both of these models consists of finding a large number of parameters. Another solution is to approximate the hysteresis by linear dynamics which can be inverted using existing linear system inversion techniques [19]. The linear approximation used in this approach inherently leads to a significant modelling error of the nonlinear hysteresis effect.

Although compensating hysteresis is well recognized to be crucial for control performance, current methods require the complicated inversion of a nonlinear hysteresis model and require an expensive identification procedure of a large number of parameters to identify the model. The aim of this paper is to exploit the dual-pair concept [20], i.e., evaluating the derivatives of the input and output, to connect the Ramberg-Osgood hysteresis model to memory elements. This facilitates both a straightforward identification procedure of only 3 parameters and a straightforward inverse that can be exploited as a feedforward controller.

The main contribution of this paper is a feedforward controller for hysteresis based on hybrid-MEM-elements. This is achieved through the following sub-contributions.

- C1 A hybrid-MEM-element is presented to model hysteresis phenomena that can be captured by the Ramberg-Osgood model, Section II.
- C2 An identification procedure of only a few parameters is introduced to identify the model parameters by exploiting the structure of a hybrid-MEM-element, Section III.
- C3 A feedforward controller to compensate the hysteresis phenomena is determined, exploiting the a straightforward inverse enabled by the structure of the hybrid-MEM-element, Section IV.
- C4 The developed approach is successfully applied to a piezoelectric actuator including a comparison to a feedforward controller based on the Prandtl-Ishlinskii model, Section V.

The present paper substantially extends preliminary results in [21], including a novel hysteresis identification approach

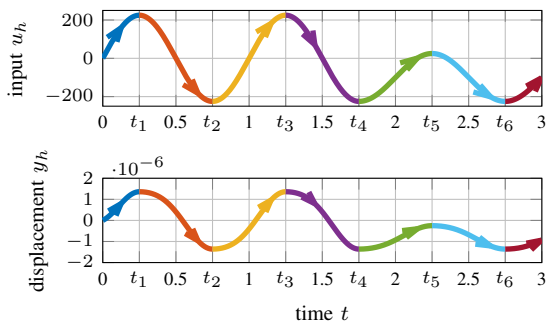

Fig. 1. Input $u_h(t)$ given by (1) and corresponding output $y_h(t)$. Each color indicates one branch of the the hysteresis loop. The time instance of each branching point is indicated by t_i.

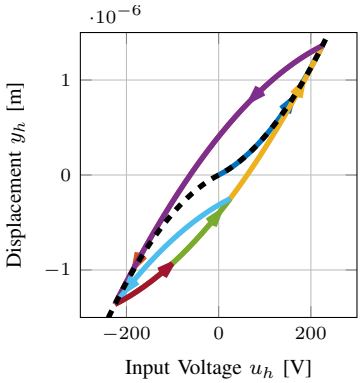

Fig. 2. Hysteresis loop when applying input signal (1). Each color indicates one branch of the the hysteresis loop. The skeleton corresponding to this hysteric behaviour is given by the dashed black line (- -). Experimental data from a piezoelectric actuator is given by crosses (+).

relevant for feedforward control, a more thorough comparison between the developed feedforward controller and present hysteresis feedforward approaches, and all proofs. Moreover, parallel to this research a hysteresis feedforward controller based on the Prandtl-Ishlinskii model is developed that allows for manual parameter tuning of many parameters, [22]. In contrast to [22], the developed feedforward controller is based on the Ramberg-Osgood hysteresis model and allows for an automated tuning approach of only a few parameters.

II. Hysteresis

In this section, the Ramberg-Osgood model, which can capture the hysteretic behaviour in piezoelectric actuators using only a few parameters, is introduced. Next, a general memory (MEM) element is introduced, which has favourable properties for both identification and its inverse. Finally, it is shown, exploiting the dual-pair concept, that the Ramberg-Osgood model in its differential form is mathematically equivalent to a memory element.

A. Modelling hysteresis

The Ramberg-Osgood model [6], [7] can capture the hysteretic behaviour in piezoelectric actuators by only a few parameters, thereby enabling contribution C2. The following example depicts a numerical simulation of the Ramberg-Osgood model, which in Section V is shown to closely resemble the response of a piezo electric actuator.

Example 1 Applying the input signal given by

$$u_h(t) = \begin{cases} 250\sin(2\pi t) & \text{if } t \leq \frac{7}{4}, \\ 125\sin(2\pi t) - 125 & \text{if } t > \frac{7}{4}, \end{cases} \tag{1}$$

leads to the signals in Fig. 1. The corresponding hysteresis loop to this behaviour is depicted in Fig. 2. Each direction change of the input signal is referred to as a branching point. Each branch between two branching points is indicated with a unique color.

The Ramberg-Osgood model is dictated by an initial skeleton curve

$$\frac{y_h}{y_h^*} = \frac{u_h}{u_h^*}\left(1 + \alpha\left|\frac{u_h}{u_h^*}\right|^{\gamma-1}\right), \tag{2}$$

where y_h is the displacement and u_h is the input signal. The material properties are characterized by the parameters $y_h^*, u_h^* \in \mathbb{R}_{>0}$, $\alpha \in \mathbb{R}_{\geq 0}$, and $\gamma \in \mathbb{R}_{>1}$. This skeleton curve is depicted by the dashed black line (- -) in Fig. 2. After the first branching point, the Ramberg-Osgood model describes the hysteretic behaviour, as follows

$$\frac{y_h - y_h^{[i]}}{2y_h^*} = \frac{u_h - u_h^{[i]}}{2u_h^*}\left(1 + \alpha\left|\frac{u_h - u_h^{[i]}}{2u_h^*}\right|^{\gamma-1}\right) \tag{3}$$

where the point $(y_h^{[i]}, u_h^{[i]}), i \in \mathbb{N}$ is the most recent point at which the direction of the input has been reversed. Each point $(y_h^{[i]}, u_h^{[i]}), i \in \mathbb{N}$ will be referred to as a branching point. Since the input signal u_h is known, the time instance of the branching points are exactly known.

B. General Memory Element

A general memory (MEM)-element, as introduced in [23], is considered

$$y(t) = M(p(t))u(t) \tag{4}$$

where $u(t)$ and $y(t)$ are the input and output signals, respectively. Here, $M : \mathbb{R} \to \mathbb{R}$ is a function of

$$p(t) = p(t_i) + \int_{t_i}^{t} g(u(\tau))\,\mathrm{d}\tau, \forall t \in [t_i, t_{i+1}) \tag{5}$$

where $g : \mathbb{R} \to \mathbb{R}$. The signal $p(t)$ represents the memory of the input, which can be interpreted as momentum, i.e., the past input integrated over time. Following the hybrid system MEM-element definition introduced in [23], the generalized momentum $p(t)$ can be reset at a time instant t_i to a value depending on $p(t_i^-)$ and $u(t_i^-)$, i.e., $p(t_i) = f(p(t_i^-), u(t_i^-))$. The time instances of the resets, $t_i, i \in \mathbb{N}$, can depend on the state and input of the system, while t_i^- represents the value of the time before the instantaneous change. This for example allows one to model a reset of the memory when the direction of the input changes, i.e., at a branching point.

All memory elements as introduced in [24] can be recovered by (4) by disregarding the reset, taking $g(u) = u$ and by

TABLE I
INPUT AND OUTPUT SIGNALS FOR THE GENERAL MEM-ELEMENT (4) TO RECOVER WELL KNOWN MEM-ELEMENTS [24]. THE CURRENT AND VOLTAGE ARE DENOTED BY $\boldsymbol{I}$ AND $\boldsymbol{V}$, RESPECTIVELY.

Element	Input u	Output y
MEMristor	I	V
MEMcapacitor	$\int_0^t I(\tau)\,\mathrm{d}\tau$	V
MEMinductor	$\int_0^t V(\tau)\,\mathrm{d}\tau$	I

a suitable choice for the input $u(t)$ and output $y(t)$. This is exemplified for the MEMristor, a resistor with a memory dependent resistance, in the example below, see Table I for other MEM-elements.

Example 2 A charge-controlled MEMristor is given by $V(t) = R(q(t))I(t)$ with V the voltage, I the current and R the resistance that depends on the charge $q(t) = \int_0^t I(\tau)\,\mathrm{d}\tau$. This MEMristor can be captured by the general MEM-element (4) by choosing input $u = I$, and output $y = V$. Moreover, $M(p) = R(p)$ with the momentum of the MEM-element given by the charge, i.e., $p = q$, which can be achieved with $g(u) = u$, and disregarding the resets.

Besides the electrical MEM-elements as introduced in [24], also mechanical memory elements can be captured by (4). Consider, e.g., the MEMdamper [25] below.

Example 3 A MEMdamper is given by $v(t) = \phi(P(t))F(t)$ with $v(t)$ the velocity, $F(t)$ the applied force, the damping constant ϕ depends on the momentum $P(t) = \int_0^t F(\tau)\,\mathrm{d}\tau$. This MEMdamper can be captured by the general MEM-element (4) by choosing input $u = F$, output $y = v$. Moreover, $M(p) = \phi(p)$ with the momentum of the MEM-element, p, given by the momentum of the damper, P, i.e., $p = P$, which can be achieved with $g(u) = u$, and disregarding the resets.

C. Modelling Hysteresis as a Hybrid-MEM-element

Next, it is shown the Ramberg-Osgood model can be written as a Hybrid-MEM-element. This is achieved by evaluating the differential input-output pair of the Ramberg-Osgood model, i.e., evaluating the mapping from $\dot{u}_h \to \dot{y}_h$ instead of $u_h \to y_h$, also referred to as the dual-pair concept [20].

One of the properties of a hybrid-MEM-element is its zero-crossing behaviour, i.e., $u = 0$ if and only if $y = 0$. From Fig. 2 it is clear that the mapping from input u_h to the output y_h of the Ramberg-Osgood model does not satisfy this property. The differential input-output pair, i.e., the mapping from $\dot{u}_h \to \dot{y}_h$, does satisfy this property, see, e.g., Fig. 3. Intuitively, this means that if the input rate changes sign, the sign of the output rate changes.

This leads to the following result, Contribution C1.

Theorem 4 *Given the hysteresis model* (3) *after its first branching point* $(y_h^{[1]}, u_h^{[1]})$ *given by* (3) *with input* $u_h(t)$*, output* $y_h(t)$ *and parameters* y_h^**,* u_h^**,* α *and* γ*. Then the input-output behaviour from the time-derivative of the input,* $\dot{u}_h(t)$*, to the time-derivative of the output,* $\dot{y}_h(t)$ *is equivalent to the hybrid-MEM-element* (4) *with* $u = \dot{u}_h$*,* $y = \dot{y}_h$*,*

$$M(p) = c_1 + c_2 p^{c_3} \tag{6}$$

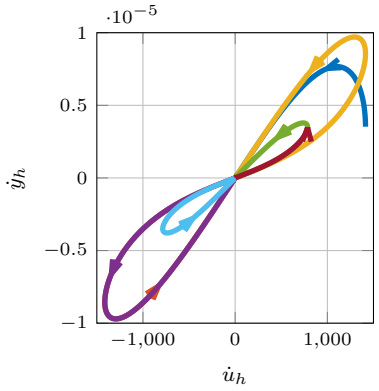

Fig. 3. Differential input-output pair of Example **??** when applying input signal (1). Each color indicates one branch of the the hysteresis loop. The skeleton corresponding to this hysteric behaviour is given by the dashed black line (- - -).

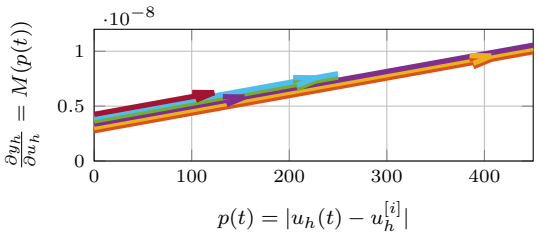

Fig. 4. The gradient $\frac{\partial y_h}{\partial u_h} = M(p(t))$ with respect to $p(t) = |u_h - u_h^{[i]}|$ corresponding to the hysteresis loop depicted in Fig. 2. To visualize the start and end point of each line all lines have a slight offset with respect to each other, in reality all lines perfectly overlap.

with $c_1 = \frac{y_h^*}{u_h^*}, \in \mathbb{R}_{>0}$*,* $c_2 = \frac{y_h^*}{u_h^*}\frac{\alpha\gamma}{(2u_h^*)^{\gamma-1}} \in \mathbb{R}_{\geq 0}$*, and* $c_3 = \gamma - 1 \in \mathbb{R}_{>0}$*. In addition, the momentum* $p(t)$ *follows from* (5) *with* $g(u) = |u|$ *and* $p(t_i) = 0$*, where* t_i *corresponds to the* i^{th} *branching point, i.e.,* $p(t) = |u_h - u_h^{[i]}|$*.*

The result of Theorem 4 is graphically represented in Fig. 4. This figure indicates that the gradient of the hysteresis loop is given by

$$\frac{\dot{y}_h}{\dot{u}_h} = \frac{\partial y_h}{\partial u_h} = M(|u_h - u_h^{[i]}|) = M(p) \tag{7}$$

with M a one-to-one mapping on the interval $[0, \infty)$. Hence, the gradient of the hysteresis loop uniquely depends on $p(t) = |u_h(t) - u_h^{[i]}|$. Moreover, at every branching point the value of $u_h^{[i]}$ is reset to u_h, i.e., at each branching point t_i, $p(t_i) = |u_h(t_i) - u_h^{[i]}| = 0$. For the input signal (1) this leads to the momentum trajectory as depicted in Fig. 4.

In the next sections, the new insights of Theorem 4 are exploited to simplify the identification of the hysteresis model and determining the inverse of the hysteresis model for a feedforward controller.

III. HYSTERESIS IDENTIFICATION EXPLOITING HYBRID MEMORY ELEMENTS

In this section, the result of Theorem 4 is exploited to introduce an identification procedure that determines the parameters of the hysteretic behaviour. First, the identification setup is introduced, for which the parameters that appear linearly

can be separated from the parameters that appear nonlinearly. Next, the procedure to identify this type of separable nonlinear least squares problems is outlined and exploited to develop an identification procedure for hysteretic behaviour.

A. Hysteresis Identification Setup

To determine a feedforward controller for a system with hysteretic behaviour, it is necessary to identify the mapping $M(p)$. To this end, consider the identification setup as depicted in Fig. 5, where the input signal is given by the momentum p and the output signal $z = \frac{\partial y}{\partial u} = \frac{\dot{y}_h}{\dot{u}_h}$. A data set $(p_i, z_i), i \in \{1, ..., m\}$, $m \in \mathbb{N}$ can be generated for this setup by performing an experiment by applying an input signal u_i, $i \in \{1, ..., m\}$ to a system with hysteretic behaviour and measuring its output $y_i \in \{1, ..., m\}$.

The undistorted output of the system $\hat{z}$ is contaminated with a noise v leading to the measurement z. Typically the position output measurement y is affected by a noise that can be considered to be white noise, and the voltage input u is not influenced by noise. The measurement noise present on the signal y will lead to a noise present in the signal z that is dependent on the velocity, i.e., at low velocities the level of the noise is relatively large compared to high velocities.

Given these signals the signals p_i and z_i can be constructed, using $p(t) = |u_h - u_h^{[i]}|$ and $z = \frac{\dot{y}_h}{\dot{u}_h}$. To obtain an approximation of the mapping M the aim is to determine the parameters c_1, c_2, and c_3 the residual between the model and data set in a least-squares sense, i.e.,

$$\arg \min_{c_1, c_2, c_3} r_M(c_1, c_2, c_3) \tag{8}$$

with the residual

$$r_M = \sum_{i=1}^{m} \left(z_i - (c_1 + c_2 p_i^{c_3})\right)^2. \tag{9}$$

B. Hysteresis Identification

The parameters c_1, c_2, c_3 in the residual (9) can be distinguished as parameters that appear linearly, i.e., c_1 and c_2, and a parameter that appears nonlinearly, i.e., c_3. Concatenating the parameters that appear linearly in a vector $a = \begin{bmatrix} c_1 & c_2 \end{bmatrix}^T$ and defining the matrix

$$\Phi(c_3) = \begin{bmatrix} 1 & p_1^{c_3} \\ 1 & p_2^{c_3} \\ \vdots & \vdots \end{bmatrix} \tag{10}$$

allows one to rewrite the residual (9) as

$$r(a, \alpha) = \|z - \Phi(c_3)a\|_2^2, \tag{11}$$

which is known as a separable nonlinear least square problem, and can be solved accordingly.

Exploiting existing results for separable nonlinear least square problems, see, e.g., [26], allows one to recast the identification problem of a Ramberg-Osgood hysteresis model to finding a single parameter, c_3, followed by an analytic solution to find the remaining parameters, constituting Contribution C2 given as follows.

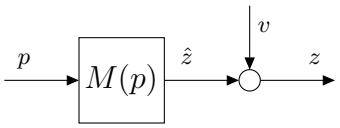

Fig. 5. Identification setup to identify the mapping $\boldsymbol{M(p)}$.

Theorem 5 *Consider the residual* (11)*, and a data set* z_i, p_i*,* $i \in \{1, ..., m\}$ *from a hysteretic element that can be described by the Ramberg-Osgood model* (6)*. The input signal* p_i *is chosen such that* $\Phi(c_3)$ *is full rank for all* $c_3 > 0$*. Then the global minimizer*

$$c_3 = \arg \min_{c_3} \|I - \Phi(c_3)\Phi(c_3)^\dagger z\|^2 \tag{12}$$

and corresponding $a = \Phi(c_3)^\dagger z$ *leads to the global minimizer of the residual* (11) *given by* $c_1 = a_1$*,* $c_2 = a_2$*, and* c_3*.*

Proof: The proof follows directly from the general result for separable least squares as elaborated on below. ■

The result of Theorem 5 shows that given a data set z_i, p_i that the hysteresis model can be identified by first solving a nonlinear optimization problem over a single parameter, and next exploiting an analytic solution to determine $a = \begin{bmatrix} c_1 & c_2 \end{bmatrix}^T$. This procedure is exploited in Section V to identify the hysteresis model that captures the hysteretic behaviour of a piezoelectric actuator. The general result for separable least squares problems that are exploited to obtain Theorem 5 are discussed below.

C. Separable Least Squares

Next, the general separable least square problems is discussed to interpret the result of Theorem 5. The general form of the residual of a separable nonlinear least square problem for a given data set $(x_i, y_i), i \in \{1, ..., m\}$ is given by

$$r(a, \alpha) = \sum_{i=1}^{m} \left(y_i - \sum_{j=1}^{n} a_j \phi_j(x_i, \alpha) \right)^2. \tag{13}$$

with unknown parameters $a = (a_1, ..., a_n)$ and $\alpha = (\alpha_1, ..., \alpha_k)$. The parameters a appear linearly in the residual $r(a, \alpha)$ and the parameters α appear nonlinearly through the functions ϕ_j, $j \in 1, .., n$.

The residual (9) can be written in the form (13) with $a_1 = c_1$, $a_2 = c_2$, $\alpha_1 = c_3$, and nonlinear functions

$$\phi_1(\alpha, i) = 1, \tag{14a}$$
$$\phi_2(\alpha, i) = p_i^{\alpha_1}. \tag{14b}$$

To write the residual (13) in matrix notation define the matrix $\Phi \in \mathbb{R}^{m \times n}$ with elements $\phi_{i,j}$ given by $\phi_{i,j}(\alpha) = \phi_j(t_i, \alpha)$. leading to the residual

$$r(a, \alpha) = \|y - \Phi(\alpha)a\|_2^2. \tag{15}$$

The following is assumed.

Assumption 6 *The matrix* $\Phi(\alpha)$ *has constant rank* $r \leq \min(m, n)$ *for* $\alpha \in \Omega_\alpha \subset \mathbb{R}^k$*,* Ω_α *the set of possible values for* α*.*

To solve the optimization problem (8), consider the residual (13) with fixed parameter vector $\alpha = \hat{\alpha}$ with $\hat{\alpha} \in \Omega_\alpha$, i.e., $r_{\hat{\alpha}}(a) = r(a, \hat{\alpha})$. Notice that finding the parameter vector a that minimizes the residual $r_{\hat{\alpha}}$ is a linear optimization problem. Hence, the optimal a is given by the Moore-Penrose inverse, i.e.,

$$\hat{a} = (\Phi(\hat{\alpha})^T \Phi(\hat{\alpha}))^{-1} \Phi^T(\hat{\alpha}) y. \tag{16}$$

The optimal solution $\hat{a}$ that minimizes $r_{\hat{\alpha}}$ is substituted in (15), i.e.,

$$r_2(\hat{\alpha}) = \|(I - \Phi(\hat{\alpha})\Phi^\dagger(\hat{\alpha}))y\|_2^2. \tag{17}$$

which solely depends on the parameter $\hat{\alpha}$.

The following relation exists between $r(a, \alpha)$ and $r_2(\alpha)$.

Lemma 7 *Consider the residual $r(a, \alpha)$ of the form (13) and its corresponding $r_2(\alpha)$ as defined by (17), and assume Assumption 6 is satisfied. Then*

1) *If $\hat{\alpha}$ is a global minimizer in Ω_α of r_2, and*

$$\hat{a} = \Phi^\dagger(\hat{\alpha}) y, \tag{18}$$

then $(\hat{a}, \hat{\alpha})$ is a global minimizer of $r(a, \alpha)$ and $r(\hat{a}, \hat{\alpha}) = r_2(\hat{\alpha})$.

2) *If $(\hat{a}, \hat{\alpha})$ is a global minimizer of $r(a, \alpha)$, then $\hat{\alpha}$ is a global minimizer of $r_2(\alpha)$ and $r(\hat{a}, \hat{\alpha}) = r_2(\hat{\alpha})$. Furthermore, if there is a unique $\hat{a}$ among the minimizing pairs of $r(a, \alpha)$, then $\hat{\alpha}$ must satisfy (18).*

For a detailed proof see [26].

This result is exploited to recast the optimization problem (8) into a nonlinear optimization problem with only a single parameter as given by Theorem 5.

D. Experimental implementation considerations

When exploiting the result of Theorem 5 on an experimental setup, both the excitation signal design and measurement noise should be carefully considered.

First, it is necessary to design the input signal u_i such that the matrix $\Phi(c_3)$ is full rank for each $c_3 > 0$ to satisfy Assumption 6. To achieve this it is sufficient to have two data points p_i which satsify $p_i \neq p_j$, $i, j \in \{1, ...m\}$. This is achieved by any signal u_i that is not constant.

Moreover, as mentioned before due to the presence of measurement noise the signal to noise ratio of the signal $z = \frac{\dot{y}_h}{\dot{u}_h}$ can become poor at low velocities, i.e., close to the branching points. Hence, only the measurement points z_i with a sufficiently large signal to noise ratio should be considered in the residual r. A user-chosen threshold on the signal-to-noise ratio determines which data points are considered in the residual.

IV. Hysteresis compensation exploiting hybrid-MEM-elements

In this section, the result of Theorem 4 is exploited to determine a feedforward controller to compensate for hysteretic behaviour. First, the feedforward controller for a general hybrid-MEM-element (19) is derived. Next, this result is exploited to determine a feedforward controller to compensate for hysteretic phenomena.

A. Feedforward Control for Hybrid-MEM-elements

The goal of the feedforward controller is to determine a control input, u_{ff}, such that the corresponding output of the system is identical to a desired output trajectory $y_d(t)$, i.e., $y(t) = y_d(t)$, for all $t \in \mathbb{R}_{\geq 0}$. The structure of a hybrid-MEM-element enables to determine the inverse system by exploiting the multiplicative inverse of the mapping M, i.e., $\frac{1}{M}$. This leads to the feedforward controller given by the following result, constituting Contribution C3.

Theorem 8 *Given a MEM-element of the form (4) with input signal $u(t)$ and output $y(t)$. Moreover, consider the feedforward controller*

$$u_{ff}(t) = \frac{1}{M(p_{ff}(t))} y_d(t) \tag{19}$$

where the momentum $p(t)$ is the solution of

$$\dot{p}_{ff}(t) = g\left(M(p_{ff}(t))^{-1} y_d(t)\right) \ \forall t \in [t_i, t_{i+1}) \tag{20}$$

with $p_{ff}(t_1) = p(t_1)$, and $p_{ff}(t_i) = f(p_{ff}(t_i^-), u_{ff}(t_i^-))$, where t_i, $i \in [2, 3, ...]$ are the reset instances, and $p_{ff}(t_i^-) := \lim_{s \uparrow t_i} p_{ff}(s)$, $u_{ff}(t_i^-) := \lim_{s \uparrow t_i} u_{ff}(s)$. For any desired output trajectory $y_d(t)$, the input signal $u_{ff}(t)$ generated by (19), applied to the MEM-element (4), leads to an output trajectory satisfying $y(t) = y_d(t)$ for all $t \in \mathbb{R}_{\geq 0}$.

Example 9 Interestingly, when applying the result of Theorem 8 for a linear equivalent of a mechanical MEM-element, the well-known feedforward components are recovered. Consider for instance the linear equivalent of the MEMdamper of Example 3, i.e., a linear damper, $v(t) = \Phi F(t)$, with v the velocity, F the force, and $\Phi \in \mathbb{R}_{>0}$ the damping constant. This linear damper can be captured by the general MEM-element (4) by choosing input $u = F$, output $y = v$, and $M = \Phi$. Exploiting Theorem 8 leads to a feedforward controller given by $F(t) = \frac{1}{\Phi} v_d(t)$ with v_d the desired velocity trajectory. This feedforward controller is equivalent to the feedforward controller to compensate viscous friction feedforward, $F = K_{fv} \frac{\mathrm{d}y_d(t)}{\mathrm{d}t}$ [3], with $\frac{\mathrm{d}y_d(t)}{\mathrm{d}t} = v_d(t)$ and $\frac{1}{\Phi} = K_{fv}$.

B. Feedforward to Compensate Hysteresis

The result of Theorem 8 leads to a straightforward feedforward controller to compensate hysteresis. Substituting the result of Theorem 4 leads to the following result.

Theorem 10 *Consider a hysteretic behaviour after its first branching point given by (3) with input $u_h(t)$, output $y_h(t)$ and parameters y_h^*, u_h^*, α and γ. Moreover, consider the feedforward controller given by*

$$\dot{u}_{hff}(t) = \frac{1}{c_1 + c_2 (p_{hff})^{c_3}} \dot{y}_{hd}(t) \tag{21}$$

where $\dot{y}_{hd}$ is the time derivative of the desired trajectory, $\dot{u}_{hff}$ the generated input rate signal, $c_1 = \frac{y_h^*}{u_h^*}$, $c_2 = \frac{\alpha\gamma}{(2u_h^*)^{\gamma-1}}$, $c_3 = \gamma - 1$ are the parameters, and the momentum

$$p_{hff}(t) = p_{hff}(t_i) + \int_{t_i}^{t} |\dot{u}_{hff}(\tau)| \, \mathrm{d}\tau \tag{22}$$

with $p_{hff}(t_i) = 0$, where t_i is the time instant of the i^{th} branching point. Applying this input rate to the piezoelectric

actuator after its first branching point with $y_h(0) = y_{hd}(0)$, *and* $u_h(0) = 0$, *leads to the output trajectory* $y_h(t) = y_{hd}(t)$ *for all* $t \in \mathbb{R}_{\geq 0}$.

Proof: Substituting the expressions for g, f and M from Theorem 4 into the feedforward controller in Theorem 8 leads to (21) and (22). ■

C. Implementation Aspects

The resets at the branching point in the feedforward controller (21) prevent the use of ordinary differential equation solvers to compute the signal $\dot{u}_{hff}$. Nevertheless, the time instances of these branching points are exactly known for a given desired trajectory y_{hd}. These time instances t_i are given by the time instances where the direction y_{hd} changes. Hence, in each of the intervals, $[t_i, t_{i+1})$ an ordinary differential equation solver can be exploited to solve the smooth nonlinear differential equation

$$\dot{p}_{hff} = |M(p_{hff})^{-1}\dot{y}_{hd}| \tag{23a}$$
$$\dot{u}_{hff} = M(p_{hff})^{-1}\dot{y}_{hd} \tag{23b}$$

with $\dot{p}_{hff}(t_i) = 0$. Solving this set of differential equations for each interval $[t_i, t_{i_1})$ results in the input signal $\dot{u}_{hff}$ which yields the output trajectory $y_h = y_{hd}$. This method is exploited in the next section to compensate for the hysteretic behaviour in a piezoelectric actuator.

V. Experimental Results

A. Experimental setup

The experimental setup used in this section is depicted in Figure 6. The actuator in this setup is a piezo stepper actuator that consist of a combination of piezoelectric elements in a configuration that propels the mover through a walking motion. The limited stroke of individual piezoelectric actuators is considered as one of their main disadvantages. The piezo-stepper actuator used in this setup maintains all advantages of the individual piezo elements, while the walking behaviour enables an unlimited stroke. To eliminate any disturbance caused by the walking motion the stroke during the experiments is limited such that only one set of piezo elements is in contact with the mover.

The piezoelectric material used in this actuator is lead zirconate titanate (PZT). The input to the actuator is a voltage in the range $[-250, 250]$ Volt. The piezoelectric actuator is connected to a mover, which is connected to a parallel guide within a frame. The position of the mover is measured by a sincos encoder with a period length of $0.5 \cdot 10^{-6}$ m, and a 16-bit digital-analog converter.

B. Identification

To identify the mapping M that corresponds to the piezoelectric actuator an open-loop experiment is performed, with an input signal $u_h(t) = 250sin(20\pi t)$. The output $y_h(t)$ is measured, and the corresponding gradient $\frac{\partial y_h}{\partial u_h}$ and generalized momentum $p_h(t) = |u_h(t) - u_h^{[i]}|$ are computed, indicated by the dots (•) in Fig. 7.

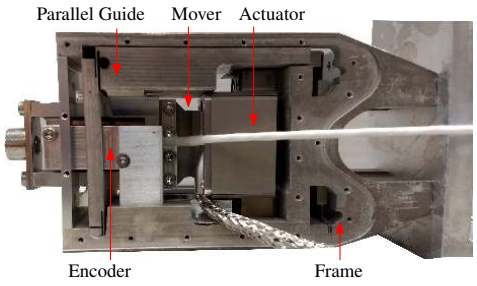

Fig. 6. Experimental setup with piezoelectric actuator.

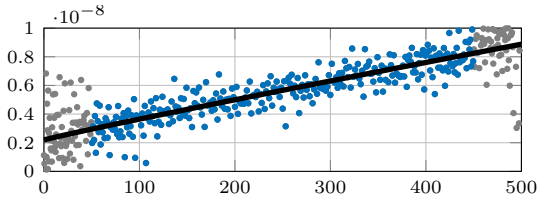

Fig. 7. Experimental data of the mapping $\boldsymbol{M(p)}$ in blue (•) and corresponding identified mapping exploiting Theorem 5 (—). The measurement points with a low signal-to-noise ratio which are not taken into account in the residual are indicated in gray (•).

To find the parameters c_1, c_2, c_3 that minimize the residual (9) the result of Theorem 5 is exploited. First, the Gauss-Newton algorithm is exploited to find the optimal parameter $\alpha_1 = c_3$ by minimizing the residual (17). Next, c_1 and c_2 are computed from (13). The resulting mapping $M(p)$ is depicted in Fig. 7.

To validate the identified model, the input signal (1) is applied to the piezoelectric actuator. In Fig. 8 the identified model is depicted together with the experimental data. This figure shows that the identified model approximates the experimental setup accurately.

C. Feedforward control

Exploiting the identified mapping $M(p)$ a feedforward controller is determined exploiting the result of Theorem 8. To validate this feedforward controller an open-loop experiment, is performed with a desired trajectory given by

$$y_d(t) = -1.6 \cdot 10^{-6}\cos(2\pi t). \tag{24}$$

Three feedforward controllers are used to generate an input signal for the piezoelectric actuator.

1) A linear feedforward controller which approximates the electric actuator by a linear spring.
2) A feedforward controller based on a Prandtl-Ishlinskii model consisting of 15 play-operators [15].
3) The developed feedforward controller (21) with the parameters c_1, c_2, and c_3 as identified in Section V-B.

The resulting position and error measurements are given in Fig. 9 and Fig. 10, respectively. From Fig. 10 it is observed that the feedforward controller (21) clearly outperforms both the linear feedforward controller, which yields an root mean square (RMS) error of 339.3 nm. This is an expected result due to the large modelling error when only a linear approximation is used. The controller based on the Prandtl-Ishlinskii model yields an RMS error of 97.5 nm, is also outperformed by the

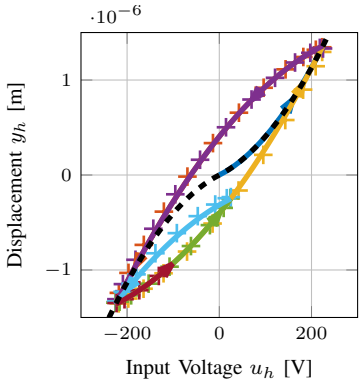

Fig. 8. Hysteresis loop when applying input signal (1). Each color indicates one branch of the the hysteresis loop. Experimental data from the piezoelectric actuator is given by crosses (+).

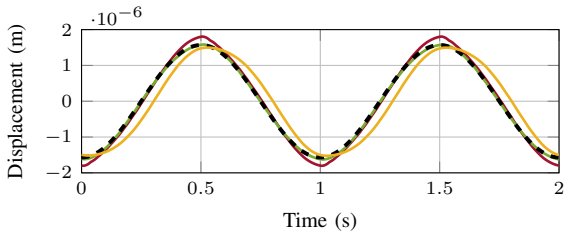

Fig. 9. Measured position of a piezoelectric actuator that aims to follow the reference trajectory depicted by the dashed line (- - -). Three feedforward controllers are compared: 1) a linear feedforward controller (—) 2) a Prandtl-Ishlinskii based feedforward controller in yellow (—), 3) the feedforward controller developed in Section IV in green (—).

feedforward controller (21) which yields the smallest RMS error of 27.9 nm, this emphasizes that even with 15 parameters the piecewise approximation of the Prandtl-Ishlinskii model does not guarantee the best performance. Moreover, the hysteresis loop from desired position y_d to measured position y, as given in Fig. 11, indicates that this relation is predominantly linear when exploiting the feedforward controller (21).

VI. Conclusion

A systematic feedforward approach that compensates for the hysteretic behaviour in piezoelectric actuators is presented exploiting a straightforward inversion of a memory-element based hysteresis model. Inspired by the dual-pair concept, it is shown how the Ramberg-Osgood model can be cast as a hybrid-MEM-element. This insight leads to both 1) a simple identification procedure that requires a nonlinear optimization over only a single parameter 2) a straightforward inverse to determine a compensating feedforward controller. Finally, the developed feedforward controller is successfully applied to a piezoelectric actuator.

Acknowledgment

The authors wish to thank Jeroen Setz, Yves Elmensdorp and Edwin Verschueren for performing the experiments.

References

[1] H. Zhong, L. Pao, and R. de Callafon, "Feedforward control for disturbance rejection: Model matching and other methods," in *2012 24th CCDC*, 2012, pp. 3528–3533.

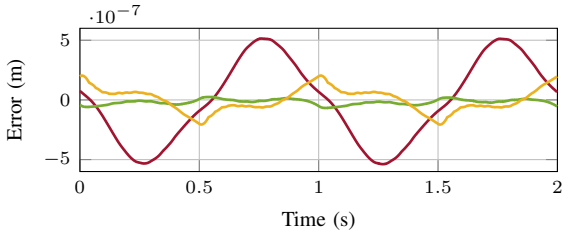

Fig. 10. Measured error of a piezoelectric actuator that aims to follow the reference trajectory (24). Three feedforward controllers are compared: 1) a linear feedforward controller (—) 2) a Prandtl-Ishlinskii based feedforward controller in yellow (—), 3) the feedforward controller developed in Section IV in green (—).

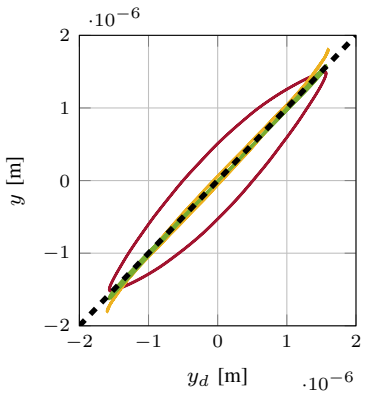

Fig. 11. Hysteresis loop from desired displacement to the measured displacement of a piezoelectric actuator. Three feedforward controllers are compared: 1) a linear feedforward controller (—) 2) a Prandtl-Ishlinskii based feedforward controller in yellow (—), 3) the feedforward controller developed in Section IV in green (—).

[2] J. Butterworth, L. Pao, and D. Abramovitch, "Analysis and comparison of three discrete-time feedforward model-inverse control techniques for nonminimum-phase systems," *Mech.*, vol. 22, no. 5, pp. 577 – 587, 2012.
[3] T. Oomen, "Control for precision mechatronics," in *Encyclopedia of Systems and Control*, J. Baillieul and T. Samad, Eds. Londen: Springer London, 2019, pp. 1–10.
[4] F. Boeren, T. Oomen, and M. Steinbuch, "Iterative motion feedforward tuning: A data-driven approach based on instrumental variable identification," *Control Eng. Pract.*, vol. 37, pp. 11 – 19, 2015.
[5] M. Ruderman and M. Iwasaki, "Observer of nonlinear friction dynamics for motion control," *IEEE Trans. on Ind. Elec.*, vol. 62, no. 9, pp. 5941–5949, 2015.
[6] W. Ramberg and W. R. Osgood, "Description of stress-strain curves by three parameters," 1943.
[7] P. C. Jennings, "Response of simple yielding structures to earthquake excitation," Ph.D. dissertation, California Inst. of Tech., 1963.
[8] M. Goldfarb and N. Celanovic, "Modeling piezoelectric stack actuators for control of micromanipulation," *IEEE Contr. Syst. Mag.*, vol. 17, no. 3, pp. 69–79, June 1997.
[9] M. Rakotondrabe, "Bouc-Wen modeling and inverse multiplicative structure to compensate hysteresis nonlinearity in piezoelectric actuators," *IEEE Trans. Autom. Sci.*, vol. 8, no. 2, pp. 428–431, April 2011.
[10] P. Ge and M. Jouaneh, "Modeling hysteresis in piezoceramic actuators," *Precision Engineering*, vol. 17, no. 3, pp. 211 – 221, 1995.
[11] R. Merry, M. Uyanik, R. van de Molengraft, R. Koops, M. van Veghel, and M. Steinbuch, "Identification, control and hysteresis compensation of a 3 DOF metrological AFM," *Asian Journal of Control*, vol. 11, no. 2, pp. 130–143, 2009.
[12] M. Al Janaideh, C.-Y. Su, and S. Rakheja, "Development of the rate-dependent Prandtl–Ishlinskii model for smart actuators," *Smart Materials and Structures*, vol. 17, no. 3, p. 035026, 2008.
[13] M. Al Janaideh, S. Rakheja, and C.-Y. Su, "A generalized Prandtl–Ishlinskii model for characterizing the hysteresis and saturation nonlinearities of smart actuators," *Smart Materials and Structures*, vol. 18, no. 4, p. 045001, 2009.
[14] V. Hassani, T. Tjahjowidodo, and T. N. Do, "A survey on hysteresis

modeling, identification and control," *Mechanical Systems and Signal Processing*, vol. 49, no. 1, pp. 209–233, 2014.
[15] K. Kuhnen, "Modeling, identification and compensation of complex hysteretic nonlinearities: A modified Prandtl-Ishlinskii approach," *European Journal of Control*, vol. 9, no. 4, pp. 407–418, 2003.
[16] M. Rakotondrabe, C. Clevy, and P. Lutz, "Complete open loop control of hysteretic, creeped, and oscillating piezoelectric cantilevers," *IEEE Trans. Autom. Sci.*, vol. 7, no. 3, pp. 440–450, 2010.
[17] M. Al Janaideh, S. Rakheja, and C.-Y. Su, "An analytical generalized Prandtl–Ishlinskii model inversion for hysteresis compensation in micropositioning control," *IEEE/ASME Transactions on mechatronics*, vol. 16, no. 4, pp. 734–744, 2010.
[18] G. Song, J. Zhao, X. Zhou, and J. A. De Abreu-Garcia, "Tracking control of a piezoceramic actuator with hysteresis compensation using inverse Preisach model," *IEEE/ASME Transactions on Mechatronics*, vol. 10, no. 2, pp. 198–209, April 2005.
[19] K. K. Leang, Q. Zou, and S. Devasia, "Feedforward control of piezoactuators in atomic force microscope systems," *IEEE Control Systems Magazine*, vol. 29, no. 1, pp. 70–82, Feb 2009.
[20] J. S. Pei, F. Gay-Balmaz, J. Wright, M. Todd, and S. Masri, "Dual input–output pairs for modeling hysteresis inspired by mem-models," *Nonlinear Dynamics*, vol. 88, no. 4, pp. 2435–2455, 2017.
[21] N. Strijbosch and T. Oomen, "Hybrid-MEM-Element feedforward: With application to hysteretic piezoelectric actuators," in *59th CDC*, 2020, pp. 934–939.
[22] N. Strijbosch, K. Tiels, and T. Oomen, "Hysteresis feedforward compensation: A direct tuning approach using hybrid-mem-elements," *IEEE Control Systems Letters*, vol. 6, pp. 1070–1075, 2022.
[23] J. S. Pei, "MEM-spring models combined with hybrid dynamical system approach to represent material behavior," *J. of Eng. Mech.*, vol. 144, no. 12, p. 04018109, 2018.
[24] M. Di Ventra, Y. V. Pershin, and L. O. Chua, "Circuit elements with memory: memristors, memcapacitors, and meminductors," *Proc. IEEE*, vol. 97, no. 10, pp. 1717–1724, 2009.
[25] M. E. Fouda, A. G. Radwan, A. S. Elwakil, and N. K. Nawayseh, "Review of the missing mechanical element: Memdamper," in *2015 IEEE International Conference on Electronics, Circuits, and Systems (ICECS)*, 2015, pp. 201–204.
[26] G. Golub and V. Pereyra, "Separable nonlinear least squares: the variable projection method and its applications," *Inverse problems*, vol. 19, no. 2, p. R1, 2003.

APPENDIX

Proof of Theorem 4: This proof consists of two steps: in the first step it is proven that the hysteric behaviour is described by the relation

$$\dot{y}_h = M(|u_h - u_h^{[i]}|)\dot{u}_h. \tag{25}$$

Next it is shown that with input $u = \dot{u}_h$ and output $y = \dot{y}_h$ the hysteric behaviour can be cast in the hybrid-MEM-element (4).

Step 1: Consider the relation between the displacement y_h and input voltage u_h given by (3) with parameters y_h^*, u_h^*, α and γ. First, the time derivative of $y_h - y_h^{[i]}$ from (3) is given by

$$\begin{aligned}
&\tfrac{\mathrm{d}}{\mathrm{d}t}(y_h - y_h^{[i]}) = \\
&\quad \tfrac{\mathrm{d}}{\mathrm{d}t}\left(\tfrac{y_h^*}{u_h^*}(u_h - u_h^{[i]})\left(1 + \alpha\left|\tfrac{u_h - u_h^{[i]}}{2u_h^*}\right|^{\gamma-1}\right)\right)
\end{aligned}$$

$$\begin{aligned}
\dot{y}_h = \tfrac{y_h^*}{u_h^*}\left(1 + \alpha\left|\tfrac{u_h - u_h^{[i]}}{2u_h^*}\right|^{\gamma-1}\right)\tfrac{\mathrm{d}}{\mathrm{d}t}\left(u_h - u_h^{[i]}\right) \\
+\tfrac{y_h^*}{u_h^*}\left(u_h - u_h^{[i]}\right)\tfrac{\mathrm{d}}{\mathrm{d}t}\left(1 + \alpha\left|\tfrac{u_h - u_h^{[i]}}{2u_h^*}\right|^{\gamma-1}\right)
\end{aligned}$$

$$\begin{aligned}
\dot{y}_h = \tfrac{y_h^*}{u_h^*}\left(1 + \alpha\left|\tfrac{u_h - u_h^{[i]}}{2u_h^*}\right|^{\gamma-1}\right)\dot{u}_h + \\
\tfrac{y_h^*}{u_h^*}\left(u_h - u_h^{[i]}\right)\alpha(\gamma-1)\left|\tfrac{u_h - u_h^{[i]}}{2u_h^*}\right|^{\gamma-2}\tfrac{|u_h - u_h^{[i]}|}{u_h - u_h^{[i]}}\tfrac{\dot{u}_h}{2u_h^*}
\end{aligned}$$

Given that $u_h^* \in \mathbb{R}_{>0}$ this equals,

$$\dot{y}_h = \tfrac{y_h^*}{u_h^*}\left(1 + \tfrac{\alpha\gamma}{(2u_h^*)^{\gamma-1}}\left|u_h - u_h^{[i]}\right|^{\gamma-1}\right)\dot{u}_h$$

This shows that the hysteresis model (3) after its first branching point can be rewritten in the form (25) with M given by (6), $c_1 = \frac{y_h^*}{u_h^*}$, $c_2 = \frac{y_h^*}{u_h^*}\frac{\alpha\gamma}{(2u_h^*)^{\gamma-1}}$, and $c_3 = \gamma - 1$.

Step 2: From the result of step 1 it is observed that by choosing $u = \dot{u}_h$, $y = \dot{y}_h$, and defining the functions g and f such that $p = |u_h - u_h^{[i]}|$ the hysteresis can be captured by a hybrid-MEM-element of the form (4). To achieve this define $g(u) = |u|$, i.e., $p(t) = p(t_i) + \int_{t_i}^{t} |\dot{u}_h(\tau)|\,\mathrm{d}\tau = p(t_i) + |u_h - u_h(t_i)|$. This shows that by taking the reset instances equal to the branching instances and $p(t_i^+) = f(p(t_i), u_h(t_i)) = 0$, $p(t) = |u_h(t) - u_h^{[i]}|$, $t \in (t_i, t_{i+1}]$, completing the proof. ■

Proof of Theorem 8: This proof consists of two steps: in the first step it is proven that the momentum of the MEM-element (4) satisfies $p(t) = p_{ff}(t), \forall t \in \mathbb{R}_{\geq 0}$ when applying the input signal (19). In the second step, it is shown that applying the feedforward signal u_{ff} as input to the MEM-element (4) leads to the output trajectory satisfying $y(t) = y_d(t), \forall t \in \mathbb{R}_{\geq 0}$.

Step 1: To show that $p(t) = p_{ff}(t), \forall t \in \mathbb{R}_{\geq 0}$ holds, consider the time derivative of (5), $\dot{p}(t) = g(u(t)), \forall t \in [t_i, t_{i+1})$ with $p(t_i) = f(p(t_i^-), u(t_i^-))$. Substitution of $u(t) = u_{ff}(t)$, with $u_{ff}(t)$ given by (19), leads to

$$\dot{p}(t) = g(M(p_{ff}(t))^{-1} y_d(t)), \forall t \in [t_i, t_{i+1}). \tag{26}$$

The right hand side of this equation is equivalent to $\dot{p}_{ff}$ given by (20). Hence, solving this equation starting from $t_1 = 0$ with $p(t_1) = p_{ff}(t_1)$ leads to

$$p(t) = p_{ff}(t), t \in [t_1, t_2). \tag{27}$$

At t_2 the value of both p and $\dot{p}_{ff}$ are reset to

$$p_{ff}(t_2) = f(p_{ff}(t_2^-), u_{ff}(t_i^-)), \text{ and} \tag{28}$$
$$p(t_2) = f(p(t_2^-), u_{ff}(t_i^-)). \tag{29}$$

From (27) it is given that $p_{ff}(t_2^-) = p(t_2^-)$, leading to $p_{ff}(t_2) = p(t_2)$. Hence, the initial condition for the differential equations defining $p_{ff}(t)$ and $p(t)$, i.e., (20) and (26), on the interval $t \in [t_2, t_3)$ are equivalent. Using this it can be proven by induction, using the same argumentation as for interval $t \in [t_1, t_2)$, that on any interval $[t_i, t_{i+1})$, $p(t) = p_{ff}(t), t \in [t_{i+1}, t_{i+1})$, thereby proving that $p(t) = p_{ff}(t), \forall t \in \mathbb{R}_{\geq 0}$ is satisfied.

Step 2: To show that $y(t) = y_d(t), \forall t \in \mathbb{R}_{\geq 0}$ holds, substitute $u = u_{ff}$, with u_{ff} given by (19), into (4), yields

$$y(t) = M(p(t))M(p_{ff}(t))^{-1} y_d(t). \tag{30}$$

Exploiting now $p(t) = p_{ff}(t), \forall t \in \mathbb{R}_{\geq 0}$, as shown in Step 1 of the proof, gives

$$y(t) = M(p_{ff}(t))M(p_{ff}(t))^{-1} y_d(t) = y_d(t) \tag{31}$$

completing the proof. ■